Applied Catalysis B: Environmental 207 (2017) 404–411

Contents lists available at ScienceDirect

Applied Catalysis B: Environmental

journal homepage: www.elsevier.com/locate/apcatb

Coral-inspired nanoscale design of porous SnS_2 for photocatalytic reduction and removal of aqueous Cr (VI)

Jiafu Qu, Dongyun Chen*, Najun Li, Qingfeng Xu, Hua Li, Jinghui He, Jianmei Lu*

College of Chemistry, Chemical Engineering and Materials Science, Collaborative Innovation Center of Suzhou Nano Science and Technology, Soochow University, Suzhou, 215123, China

ARTICLE INFO

Article history:
Received 31 October 2016
Received in revised form 18 January 2017
Accepted 13 February 2017
Available online 14 February 2017

Keywords:
SnS_2 nanocrystals
Macroporous silica
Photocatalytic reduction
Cr (VI) removal

ABSTRACT

Frequent industrial discharge of various contaminants such as heavy metals into water resources has caused severe environmental damage. In this study, a unique porous corallite-like nanocomposite (SPNH-MOSF@SnS_2) was successfully fabricated *via* surface modification of visible-light-driven photocatalyst (SnS_2) and chelating ligand (spirobenzopyran derivative, SPNH) on macroporous ordered siliceous foam (MOSF). In our approach, SnS_2 was selected as the photocatalyst due to its high visible light induced photocatalytic activity. SPNH was modified because it could selectively chelate soluble Cr (III) when exposed to ultraviolet light. This unique nanocomposite could be used for highly efficient reduction and removal of hexavalent chromium [Cr (VI)] from wastewater, especially under the mildly acidic condition. The results indicate encouraging applications of this as-prepared new nanocomposite for treating Cr (VI) containing wastewater.

1. Introduction

As chromium (Cr) and its compounds have been widely used in the smelting, electroplating, leather and paint areas [1–3], their pollution to the environment is becoming more and more serious. Cr mainly exits as Cr (VI) and Cr (III), the former is much more harmful to human health [4–7]. Due to the high toxicity and high mobility of Cr (VI) in water, Cr containing wastewater has always been a severe issue in wastewater treatment. Various disposal methods have been exploited to treat Cr (VI), such as chemical reduction, ion exchange, bacterial degradation, adsorption and photocatalytic reduction [8–17]. Among these methods, technologies of reducing Cr (VI) to Cr (III) in wastewater has been studied extensively. This is because Cr (III) in water could be precipitated as $Cr(OH)_3$ in neutral or alkaline condition [18,19]. However, to the best of our knowledge, soluble Cr (III) still has strong toxicity to aquatic species [20–22]. It is worth noting that Cr (III) might be oxidized to Cr (VI) by some bacteria [22]. In this context, to prevent the aquatic lives from suffering toxic soluble Cr (III) and maintain the ecological balance, we have to focus on developing new materials that not only can remove Cr (VI) but also can remove Cr (III) efficiently.

In the past few years, much attention has been attracted to utilize photocatalytic techniques to solve environmental pollutions [23–25]. Since they are efficient, cost-effective, and do not need any perilous chemicals, photocatalysts such as TiO_2[26–29], CdS [30,31], ZrO_2[32], ZnO [33,34] and SnS_2[5,35,36] have been widely employed in dealing with water or air pollution issues. Among the above-mentioned photocatalysts, SnS_2 has received significant attention due to its unique optical properties [5,35]. Many studies have proved the reduction of Cr (VI) using SnS_2 under visible light irradiation and results showed that it can reduce Cr (VI) with high efficiency and more time-saving when compared with other methods [20,35]. Furthermore, the nanocrystals had also been confirmed that it can adsorb Cr (III) [35].

Porous materials that possess large surface area and specific pore volume have gained considerable interests due to their potential applications as adsorbents or catalyst supports [37,38]. Porous silica is a well-known material because it can be modified easily and used as adsorbent. In this work, we successfully fabricated a unique polyporous corallite-like nanocomposite in order to remove water-soluble Cr ions. Macroporous ordered siliceous foams (MOSF) which has large pores was selected as matrix to encapsulate SnS_2 nanocrystals for reducing Cr (VI) under visible-light irradiation. In addition, we decorated a spirobenzopyran derivative (SPNH) on the surface of MOSF, which can chelate soluble Cr (III) when it was exposed to UV-light [39]. Because of the SnS_2 and SPNH modification, the obtained functional nanocompos-

* Corresponding author.
E-mail addresses: dychen@suda.edu.cn (D. Chen), lujm@suda.edu.cn (J. Lu).

http://dx.doi.org/10.1016/j.apcatb.2017.02.050
0926-3373/

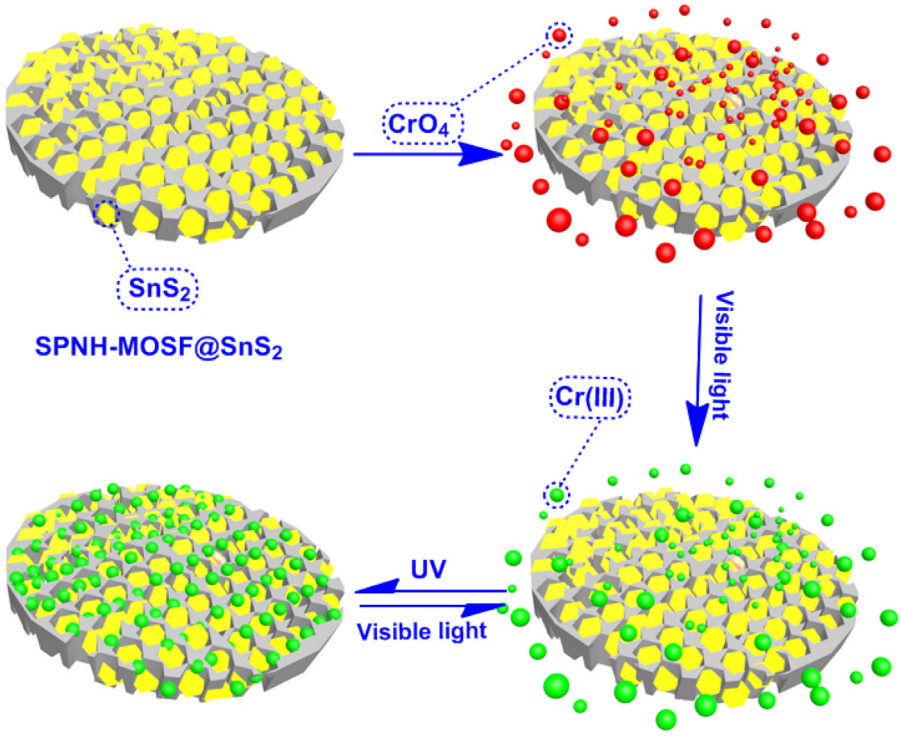

Scheme 1. Illustration of the reduction and removal process of SPNH-MOSF@SnS_2 for Cr (VI).

ite showed excellent ability of photocatalytic reduction and Cr ions adsorption. The as-prepared functional nanocomposite with both photocatalytic reduction and adsorption properties was abbreviated SPNH-MOSF@SnS_2, and the treatment process of Cr ions containing wastewater was illustrated in Scheme 1.

2. Experimental section

2.1. Materials

All chemicals were used as received without further purification. $EO_{20}PO_{70}EO_{20}$ (P123, where EO is poly-(ethylene oxide) and PO is poly-(propylene oxide)) was purchased from Sigma-Aldrich. Tetramethyl orthosilicate (TMOS), $SnCl_4{\cdot}5H_2O$, thioacetamide (TAA) and other chemicals were of analytic grade and purchased from the Sinopharm Chemical Reagents Co., Ltd.

2.2. Instrumentation

Transmission electron microscopy (TEM; Hitachi H600) and scanning electron microscopy (SEM; Hitachi S-4800) coupled with X-ray energy dispersive spectroscopy (EDS) were used to observe the structure, size and morphology in the fabrication process of SPNH-MOSF@SnS_2. X-ray diffraction (XRD; X' Pert-Pro MPD) and Fourier transform infrared spectroscopy (FT-IR; Nicolet 4700) were employed to represent the effect of SnS_2 loading and modification of carboxyl on MOSF, respectively. The elemental mapping images were measured by FEI Tecnai F-20 High Resolusion TEM (HRTEM) and the BET surface area was analyzed by BET theory. Electrochemical measurements were conducted with a CHI 660B electrochemical system (Shanghai, China) with a standard three-electrode cell, Pt plate and Ag/AgCl electrode was used as the counter electrode and the reference electrode, respectively. The composition analyses of HOOC-MOSF@SnS_2 and SPNH-MOSF@SnS_2 were determined by X-ray photoelectron spectra (XPS; Axis Ultra HAS). The optical properties were determined by UV–vis diffuse reflectance spectroscopy (UV-vis DRS, Shimadzu UV-3600).

2.3. Preparation of MOSF@SnS_2

The MOSF material was synthesized according to the previous literature [40]. Typically, 1.0 g P123 and 1.7 g Na_2SO_4 were dissolved in 30 g of NaAc-HAc buffer solution (pH = 5, C_t = 0.02 mol/L, where $C_t = C_{NaAc} + C_{HAc}$) to form a homogenous solution. Then 1.52 g TMOS was added to this solution under stirring. After 5 min, stirring was stopped. Subsequently, the mixture solution was transferred to a stainless-steel autoclave and kept statically for 24 h. Then, the autoclave was heated at 100 °C for another 24 h. The precipitates were filtered and washed with water several times. Whereafter, the white solid were dried at room temperature. The final MOSF products were obtained by calcination at 550 °C for 5 h.

MOSF@SnS_2 nanocrystals were prepared as follows. In brief, 500.0 mg MOSF, 1.753 g $SnCl_4{\cdot}5H2O$ and 1.052 g citric acid were dissolved in 40 mL water under stirring, and subsequently 751.3 mg TAA were added in the aqueous solution. Then, the mixture was transferred into a stainless-steel autoclave of 50 mL capacity and heated at 150 °C for 12 h the yellow precipitates were filtered, washed with deionized water, and dried in vacuum at 100 °C for 4 h. The produced solid were designated as MOSF@SnS_2 nanocrystals. Pristine SnS_2 nanocrystals were prepared as the same method described above but without MOSF.

2.4. Preparation of SPNH-MOSF@SnS_2

To a dispersion of MOSF@SnS_2 (200 mg) in 100 mL acetonitrile, 3.0 mL 3-(aminopropyl) triethoxysilane (KH550) were added. Then the mixture was kept overnight with vigorously stirring at room temperature. After the reaction, the yellow solid were separated out, washed with ethanol and redispersed in 20 mL DMF under stirring, followed by addition of a mixture containing 1.5 g succinic anhydride and 20 mL DMF. After stirred for 24 h, the solid

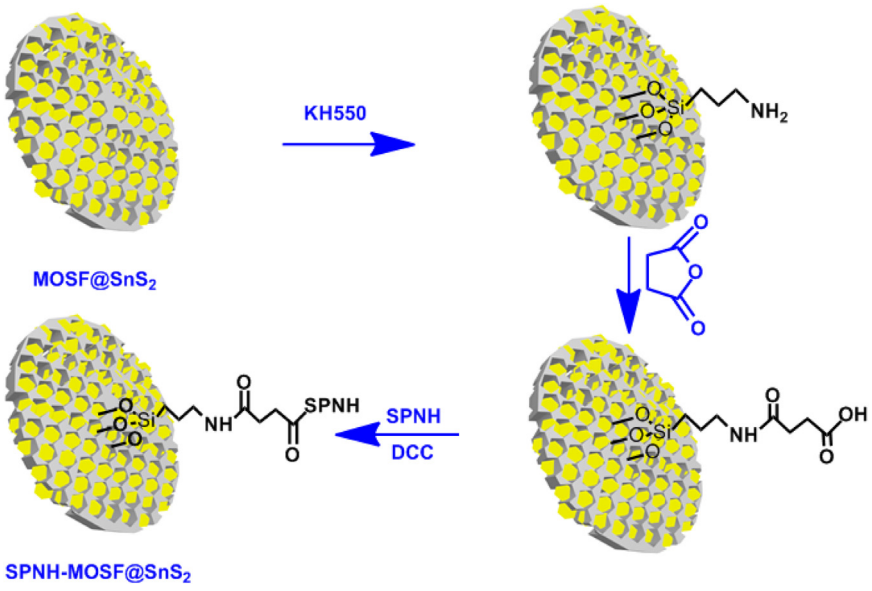

Scheme 2. Illustration of the synthetic procedure of SPNH-MOSF@SnS_2.

powder was separated out and washed with ethanol, then dried in vacuum at 60 °C. The resulting yellow solid was denoted as HOOC-MOSF@SnS_2.

The synthesis route of compound SPNH is shown in Scheme S1. (See details in Supporting Information). SPNH-MOSF@SnS_2 was prepared as the literature described [41]. In brief, 200 mg HOOC-MOSF@SnS_2 was dispersed in 100 mL dichloromethane. Afterward, 6.0 g SPNH and 3.0 g N, N-dicyclohexylcarbondiimide (DCC) were added under argon atmosphere. Then the reaction mixture was stirred at room temperature for 24 h. Finally, the solid products were collected, washed with ethanol for several times, and dried at 60 °C. This obtained yellow powder was denoted as SPNH-MOSF@SnS_2. The fabrication process of SPNH-MOSF@SnS_2 is shown in Scheme 2.

2.5. Photocatalytic reduction of Cr (VI)

Cr (VI) mainly exists in forms of $Cr_2O_7^{2-}$ in water [20], so we use potassium dichromate solution to imitate Cr (VI)-containing wastewater. To qualitatively investigate the visible light catalytic ability of SPNH-MOSF@SnS_2, 50 mL $K_2Cr_2O_7$ solutions at different concentrations (50, 70, 100 mg/L) were poured into transparent glass bottles separately, and then 50 mg of SPNH-MOSF@SnS_2 were added to each bottle. The mixtures were stirred and irradiated by Xe lamp (300 W, λ > 400 nm), respectively. Measure UV–vis spectrum at regular intervals until the Cr (VI) was completely reduced and the spectra no longer changed. Minutes of completely catalytic reduction were compared to analyze the abilities of visible light catalytic reduction.

In order to study the effect of pH on the catalytic efficiency, 50 mg SPNH-MOSF@SnS_2 were added to 50 mg/L $K_2Cr_2O_7$ solutions at various pH values (2, 4, 8). Then these solutions were stirred and irradiated by Xe lamp (300 W, λ > 400 nm), respectively. Measure UV–vis spectrum by UV–vis spectrophotometer at regular intervals until the spectra no longer changed. Minutes of completely reduction were compared to assess the effect of pH values.

2.6. Removal of total chromium

To quantificationally evaluate the catalytic effect of SPNH-MOSF@SnS_2, 50 mg of SPNH-MOSF@SnS_2 were firstly added to 50 mL of $K_2Cr_2O_7$ solutions prepared in different initial concentrations (10, 20, 30, 40, 50, 70, 100 mg/L). Then pH of each solution was adjusted to neutral and it was irradiated by Xe lamp (300 W, λ > 400 nm) with stirring for 90 min. After reaction, the concentrations of unreduced Cr (VI) in solutions were determined respectively by using a colorimetric method of 1, 5- diphenylcarbazide spectrophometry [20,37]. Second, 50 mg of SPNH-MOSF@SnS_2 were respectively used to reduce various concentrations of $K_2Cr_2O_7$ solutions (10, 20, 30, 40, 50, 70, 100 mg/L) under irradiation by using Xe lamp (300 W, λ > 400 nm) for 90 min, then these solutions were moved to be exposed to ultraviolet light for 10 min. After adsorption, solids were separated from aqueous solutions and the concentrations of total chromium in solutions were analyzed by atomic absorption spectroscopy (AAS). Third, the SPNH-MOSF@SnS_2 which had been used for photocatalytic reduction-adsorption completely was analyzed by XPS to determine the valance state of chromium adsorbed on SPNH-MOSF@SnS_2.

Comparative experiments were carried out as follows, 50 mg of diverse materials (SPNH-MOSF@SnS_2, SnS_2, MOSF) were added to 50 mg/L of $K_2Cr_2O_7$ solutions (where $C_{Cr(VI)}$ = 17.68 mg/L) severally. Then each was irradiated by Xe lamp (300 W, λ > 400 nm) with stirring for 90 min. After irradiating by visible light, each was moved to be irradiated by ultraviolet light for 10 min. At last, total chromium in solutions were analyzed by AAS to compare removal effect.

3. Results and discussion

The structure and morphology of MOSF and MOSF@SnS_2 were analyzed by TEM. As shown in Fig. 1a, the MOSF showed a foam-like porous microstructure. The microstructure of MOSF was further observed by TEM using ultrathin sectioning technique. As shown in Fig. 1b, MOSF had high pore volumes and the pore diameter was about 100 nm. The pristine SnS_2 nanocrystals were also characterized by TEM (Fig. S1), the SnS_2 nanocrystals were lamellate with a size of about 20 nm. Fig. 1c showed the TEM image of MOSF@SnS_2, the macroporous foam-like structure of MOSF was still maintained after the encapsulation of SnS_2 nanoplates. From TEM slices image of MOSF@SnS_2 in Fig. 1d, SnS_2 nanoplates were observed clearly loaded in the pores of MOSF.

Fig. 2a and b were SEM images of MOSF@SnS_2. As shown in Fig. 2a, the rough surface of MOSF@SnS_2 was infested with pores

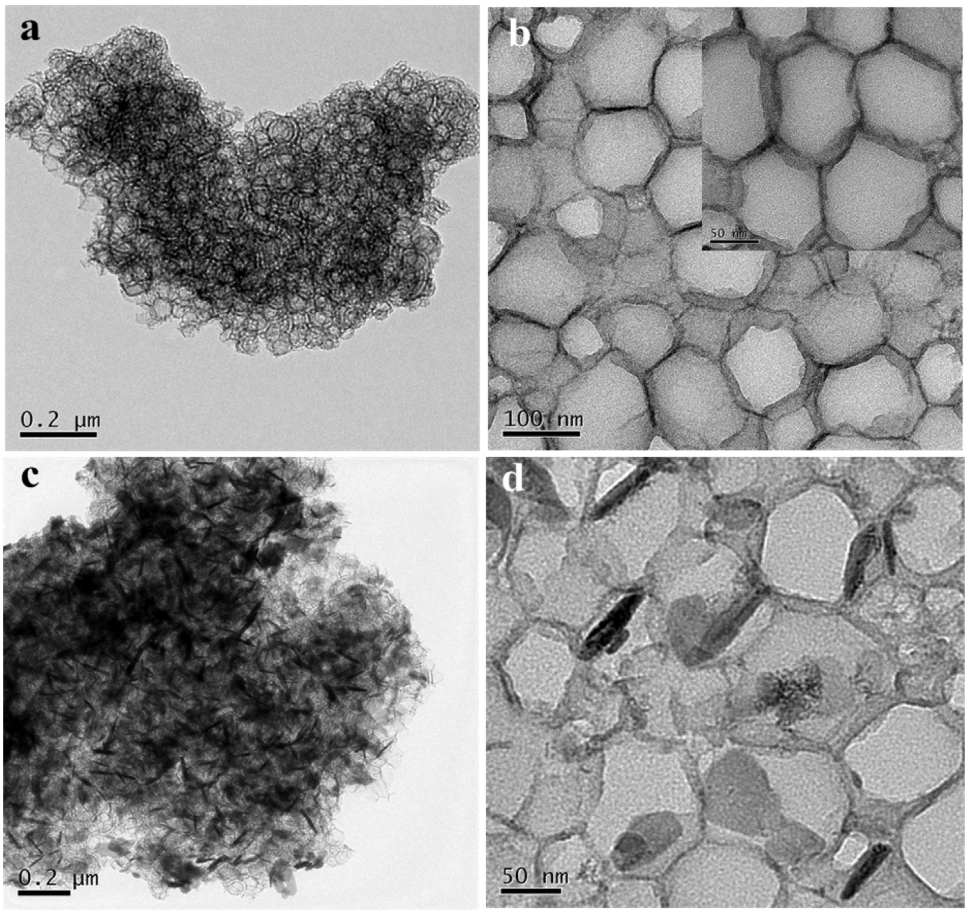

Fig. 1. TEM images of MOSF (a), MOSF@SnS_2 (c); TEM slices images of MOSF (b). Inset: TEM slices images of MOSF at high magnification. TEM slices images of MOSF@ SnS_2 (d).

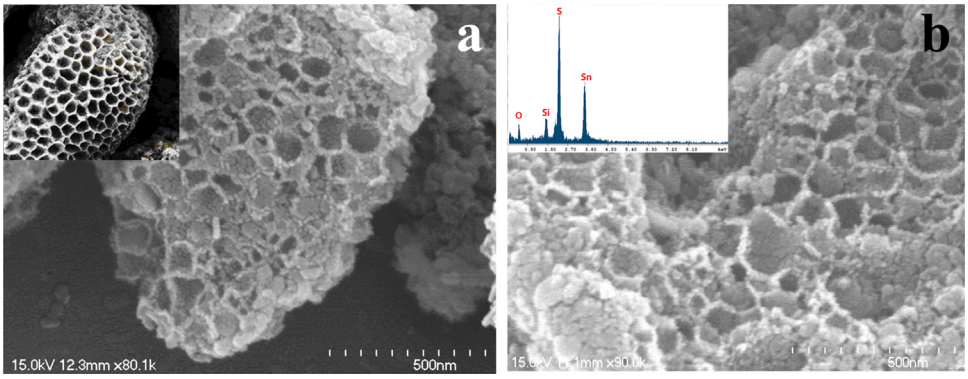

Fig. 2. SEM images of MOSF@SnS_2 at low magnification (a), at high magnification (b). Inset: photograph of corallite (a), EDS spectra of MOSF@SnS_2 (b).

which like the porous corallite. The detailed morphology of surface of MOSF@SnS_2 was shown in Fig. 2b, which revealed that lots of SnS_2 nanoplates can be seen in the "corallite". Inset in Fig. 2b was EDS spectra, which demonstrated that certain amounts of SnS_2 were existed in MOSF. The detailed elemental mappings of MOSF@SnS_2 were shown in Fig. S2, the results clearly revealed the presence and uniform distribution of SnS_2 in MOSF. Same characterization results can be seen in XRD patterns (Fig. 3a). From XRD patterns, the diffractional peaks indicative of SiO_2 and SnS_2 can be displayed in MOSF@SnS_2. The XRD patterns of MOSF, SnS_2 and MOSF@SnS_2 in Fig. 3a further confirmed that the SnS_2 nanoplates were loaded in successfully. The small-angle XRD of MOSF and MOSF@SnS_2 curves were shown in Fig. S3. As shown in Fig. S3, there was an obvious peak at 0.148°. According to the formula of Debye-Scherrer, the average pore size of the materials was calculated as ~59.7 nm. The electrochemical behavior of MOSF@SnS_2 was shown in Fig. S4. As can be seen, a strong photocurrent for MOSF@SnS_2 was generated and noticeable photocurrent responses were clearly observed, which confirmed photocatalysis properties of the catalyst.

The Nitrogen adsorption-desorption isotherms of MOSF, MOSF@SnS_2 and the corresponding pore-size distribution are shown in Fig. S5. The Brunauer-Emmett-Teller (BET) surface area are 234.53 and 103.85 $m^2\,g^{-1}$, respectively. The considerable decrease in BET surface could be attributed to the successful loading of SnS_2 in pores of MOSF. As shown in Fig. S5, the macroporous

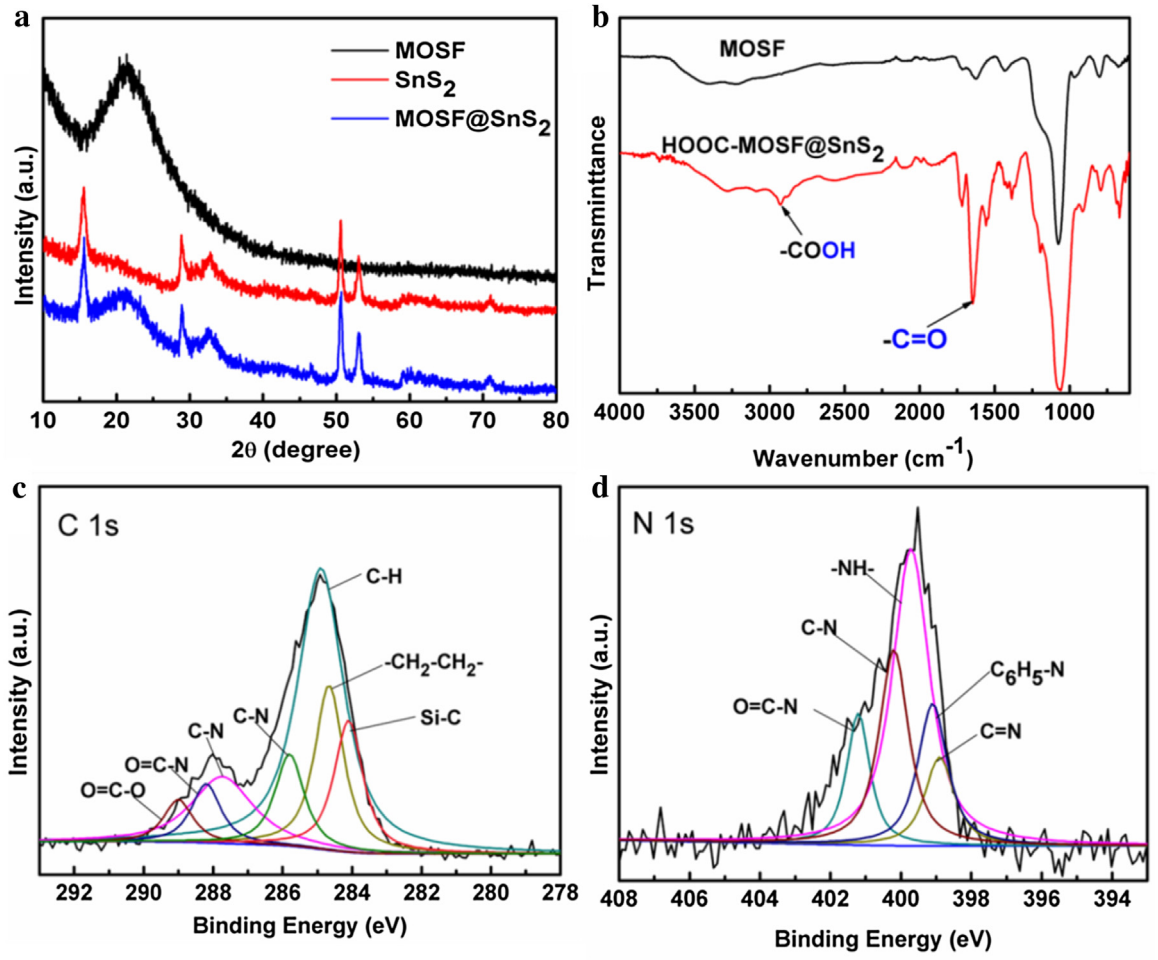

Fig. 3. XRD patterns of MOSF, SnS_2 and MOSF@SnS_2 (a), FT-IR spectra of MOSF and HOOC-MOSF@SnS_2 (b), C 1s XPS spectra of HOOC-MOSF@SnS_2 (c), N 1s XPS spectra of SPNH-MOSF@SnS_2 (d).

structure was revealed due to the capillary condensation occurs at relatively higher P/P_0 close to 1.0. The inset in Fig. S5 were pore-size distribution, from it shown the pore size distribution is mainly among 0–60 nm.

FT-IR spectra of MOSF and HOOC-MOSF@SnS_2 were displayed in Fig. 3b. The peak observed at 3423 cm^{-1} and 1101 cm^{-1} were characteristic of the Si—OH and Si—O—Si vibration respectively. After KH550-COOH modification, Si—OH vibration peak at 3423 cm^{-1} significantly decreased and the Si—O—Si bond vibration peak at 1101 cm^{-1} significantly increased, this phenomenon indicated that part of KH550-COOH and Si—OH had a condensation reaction. There were new peaks at 2931 and 2855 cm^{-1}, which could be attributed to the methylene stretching vibrations of modifiers [42]. New peak at 1379 cm^{-1} was attributable to the secondary amide —CO—NH— absorption band. The above analysis showed that the modifier (KH550-COOH) was successfully grafted onto the surface of MOSF.

The modification of carboxyl was further confirmed by XPS spectra. High resolution XPS spectrum of C1 s of HOOC-MOSF@SnS_2 was shown in Fig. 3c. The evolution of C1 s with seven peaks were observed at about 283.8, 284.6, 285.0, 285.8, 287.7, 288.2, and 289.0 eV, which could be ascribed to carbon atoms in Si-C, $-CH_2-CH_2-$, C—H, C—N, C—N in KH550, O═C—N and O═C—O in carboxyl groups. From the appearance of O═C—O, modification of carboxyl groups was verified. Decoration of SPNH onto MOSF was also characterized by XPS, the N1 s XPS spectrum of SPNH-MOSF@SnS_2 was shown in Fig. 3d. The N1 s spectrum can be well fitted into five peaks at 398.9, 399.1, 399.8, 400.2, and 401.2 eV, which could be attributed to N in C═N, C_6H_5—N, —NH—, C—N, and O═C—N respectively. C═N and C_6H_5—N were only derived from molecule of SPNH. Hence, the results could prove that SPNH were successfully grafted.

UV-vis DRS was measured and converted into absorption spectra to study the light absorption properties of SnS_2 and SPNH-MOSF@SnS_2 (Fig. 4a). As shown in Fig. 4a, SnS_2 displayed photoabsorption performance in visible light region. After SnS_2 loading and SPNH modification on MOSF, SPNH-MOSF@SnS_2 still showed a wide light absorption wave length which ensured that this new material was capable of harvesting visible light. The Tauc approach [5] was invoked to determine the band gap energy (E_g) of SPNH-MOSF@SnS_2 and the result was shown in Fig. 4b, the band gap of SPNH-MOSF@SnS_2 obtained from Fig. 4b was about 2.1 eV. The low band gap suggested that SPNH-MOSF@SnS_2 exhibited visible light driven photocatalytic ability.

To investigate the photo-catalysis capability of SPNH-MOSF@SnS_2, tests were conducted. UV–vis spectra in Fig. 5 revealed that with the increase of $K_2Cr_2O_7$ concentration, photocatalytic reduction ability is reduced. Typically, to achieve a complete reduction of 50 mg/L $K_2Cr_2O_7$ solution, SPNH-MOSF@SnS_2 should be exposed to visible light for nearly 85 min (Fig. 5a). But for 70 mg/L and 100 mg/L, 120 min and 210 min were required severally (Fig. 5b and c). It is summarized that photocatalytic activity decreased as the concentration of Cr (VI) increased.

pH is one of the most parameters affecting photocatalysis [5,43]. Fig. 6 showed the effects of pH on photocatalysis reduction of Cr (VI)

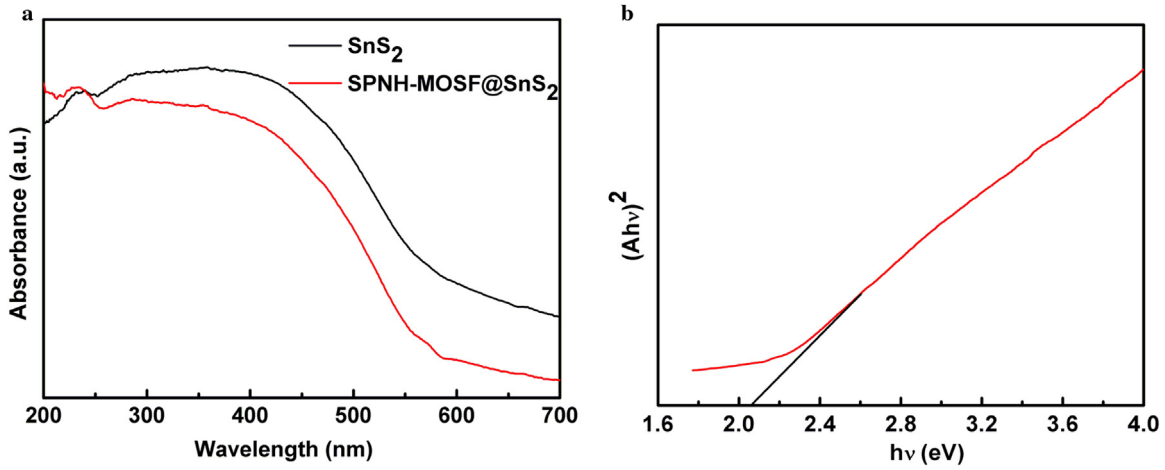

Fig. 4. UV–vis DRS spectra of SnS_2 and SPNH-MOSF@SnS_2 (a), corresponding band gap of SPNH-MOSF@SnS_2 (b).

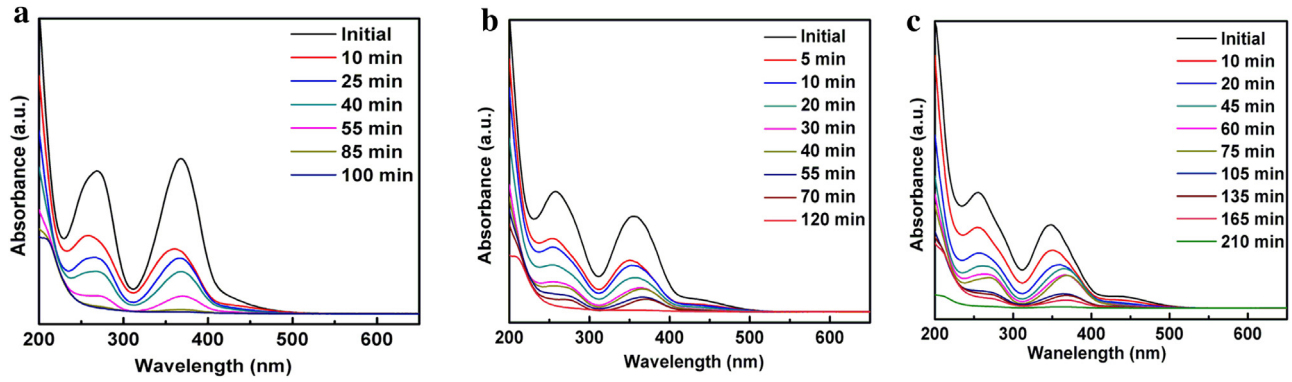

Fig. 5. Time dependence of the UV–vis spectra in photocatalytic reduction of 50 mL various concentration of $K_2Cr_2O_7$ solution in presence of 50 mg SPNH-MOSF@SnS_2: 50 mg/L (a), 70 mg/L (b), 100 mg/L (c).

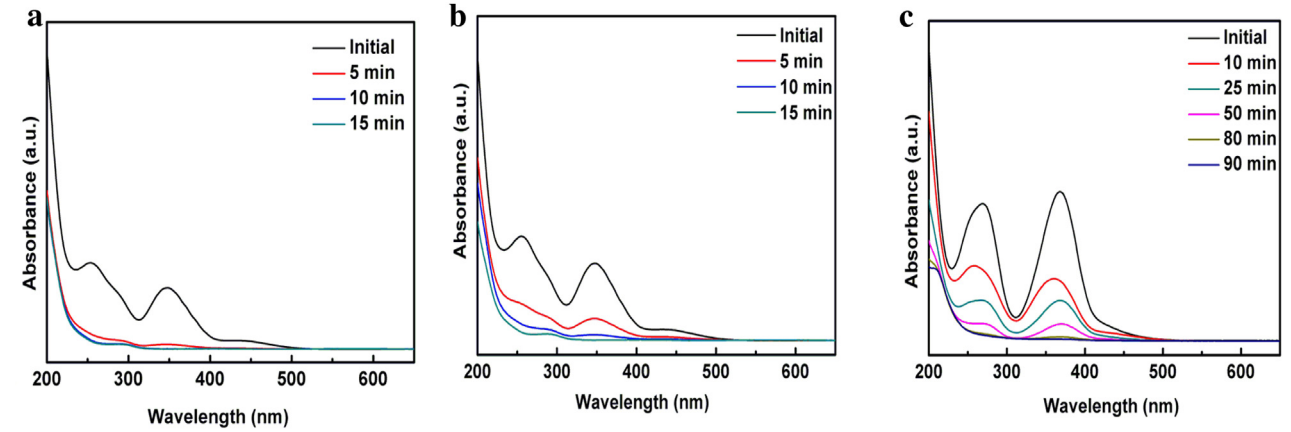

Fig. 6. Photocatalytic reduction of 50 mL of 50 mg/L $K_2Cr_2O_7$ solution under visible light in the presence of 50 mg SPNH-MOSF@SnS_2 at different pH values: 2 (a), 4 (b), 8 (c).

by SPNH-MOSF@SnS_2. It was observed that photocatalytic reduction of soluble Cr (VI) in low pH condition was much higher than that in high pH condition. This expression resulted from the fact that at high pH condition, the deposition of $Cr(OH)_3$ increased and attached to the surface of SPNH-MOSF@SnS_2 caused a decrease in photocatalytic activity.

Fig. 7a reflected the photocatalytic reduction efficiencies of 50 mg SPNH-MOSF@SnS_2 exposed to visible light for 90 min at different initial $K_2Cr_2O_7$ concentrations. It can be seen clearly that the "corallite" (SPNH-MOSF@SnS_2) could reduce Cr (VI) with a high efficiency. Typically, for 10, 20 and 30 mg/L $K_2Cr_2O_7$ solutions, the photocatalytic efficiencies were almost 100%. Even when the $K_2Cr_2O_7$ concentration was 100 mg/L, catalytic efficiency also reached more than 95%. As shown in Table 1, SPNH-MOSF@SnS_2 showed excellent photocatalytic performance when compared with other traditional visible photocatalysts. Fig. 7b revealed the total Cr removal efficiencies of 50 mg "corallite" exposed to visible light and ultraviolet light successively at different initial $K_2Cr_2O_7$ concentrations. The removal efficiencies were still high, which declared that the Cr (III) was adsorbed by the "corallite" under

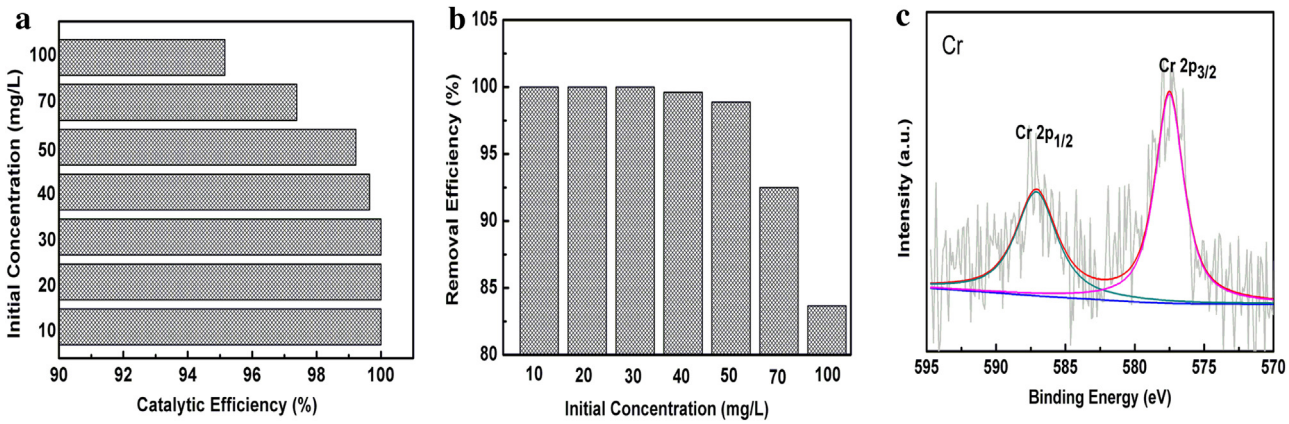

Fig. 7. Photocatalytic reduction efficiencies of 50 mg SPNH-MOSF@SnS_2 exposed to visible light for 90 min at different initial $K_2Cr_2O_7$ concentrations (a), total chromium removal efficiencies of 50 mg SPNH-MOSF@SnS_2 exposed to visible light and ultraviolet light successively at different initial $K_2Cr_2O_7$ concentrations (b), Cr XPS spectra of SPNH-MOSF@SnS_2 which had been employed for completely reduction-adsorption (c).

Table 1
Comparison of photocatalytic Cr (VI) reduction results.

Systems	pH	Catalyst dosage (mg/mL)	$[Cr(VI)]_0$(mg/L)	Time (min)	Removal efficiency (%)	Reference
SPNH-MOSF@SnS_2	7	1	50	90	99.5	Our work
	7	1	100	90	95	
TiO_2	2	1	10	300	80	[29]
ZnO	7	1	15	120	78	[34]
ZnO-TiO_2	3	1	20	120	100	[33]

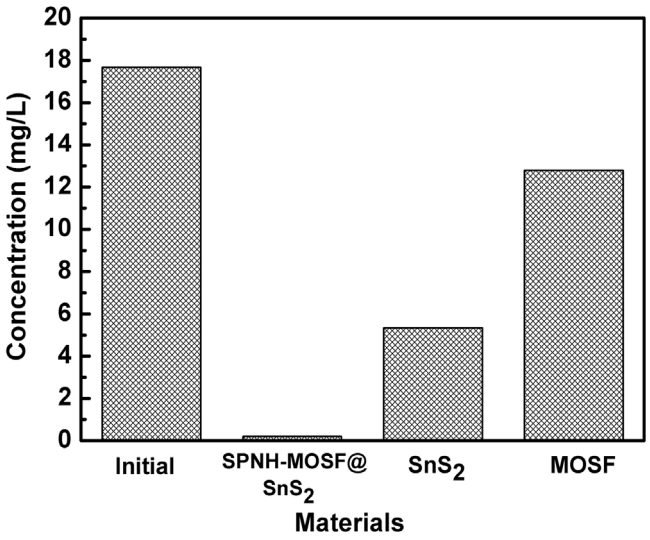

Fig. 8. Concentration of total chromium in solution after reduced by different materials.

UV light irradiation. This is because the surface of "corallite" decorated with SPNH would generate a phenoxy group by ring opening reaction when exposed to UV light, and the phenoxy group could selectively chelate soluble Cr (III) via ligand coordination. To 100 mg/L of $K_2Cr_2O_7$ solutions, the "corallite" could remove 84% of Cr ions. Fig. 7c was the Cr XPS spectra of SPNH-MOSF@SnS_2 which had been utilized for photocatalytic reducing and adsorbing Cr. Two distinct peaks at 586.3 eV and 576.8 eV representing Cr^{3+} 2p1/2 and Cr^{3+} 2p3/2 respectively were observed from Fig. 7c, which indicated that chromium adsorbed on "corallite" was Cr (III) state. Test of visible light catalyzing 50 mg/L $K_2Cr_2O_7$ solution for 30 min and adsorbing for 10 min under UV light by SPNH-MOSF@SnS_2 was conducted, and the Cr XPS was also analyzed (Fig. S6). From Fig. S6, peak at 580.82 eV which belong to Cr (VI) in $K_2Cr_2O_7$ was observed. That signified the Cr (VI) was not completely reduced and adsorbed onto the "corallite". The XPS result in Fig. 7c implied that Cr (VI) was completely reduced into Cr (III) and Cr (III) was adsorbed onto "corallite".

To prove the stability of photocatalyst, the degradation cycles of Cr (VI) solution (50 mg/L, 50 mL) was shown in Fig. S8. As can be seen, the photocatalyst showed a good catalytic activity after 3 cycles, implying the excellent cycling performance in degrading Cr (VI) from wastewater. To compare the removal efficiency of SPNH-MOSF@SnS_2 with that of other two materials, the comparative experiments were conducted. As shown in Fig. 8, the concentration of $K_2Cr_2O_7$ solution after photocatalytic reduction-adsorption by SPNH-MOSF@SnS_2 was as low as 0.2 mg/L, but the other two concentrations were much higher, which suggested that the "corallite" was superior to the other materials in removing Cr (VI).

4. Conclusions

A unique porous corallite-like nanocomposite (SPNH-MOSF@SnS_2) was fabricated to reduce and remove Cr (VI). This new material used MOSF as the matrix. Due to SnS_2 and SPNH modification, the "corallite" exhibited high visible-light catalytic activity and high adsorption capacity under UV light irradiation. The "corallite" could reduce soluble Cr (VI) very quickly especially under the condition of low pH. This new composite can reduce and remove Cr (VI) from $K_2Cr_2O_7$ solution whose concentration was less than 50 mg/L with an efficiency of nearly 100%. In summary, SPNH-MOSF@SnS_2 exhibits great ability in removing Cr (VI) and has encouraging potential applications for treating Cr (VI)-containing water.

Acknowledgements

We gratefully acknowledge the financial support provided by National Natural Science Foundation of China (21336005, 21301125, and 51573122), Natural Science Foundation of the Education Committee of Jiangsu Province (15KJB150026), Envi-

ronmental Protection Research Foundation of Suzhou, and Suzhou Nano-project (ZXG2013001, ZXG201420).

Appendix A. Supplementary data

Supplementary data associated with this article can be found, in the online version, at http://dx.doi.org/10.1016/j.apcatb.2017.02.050.

References

[1] L. Chai, S. Huang, Z. Yang, B. Peng, Y. Huang, Y. Chen, J. Hazard. Mater. 167 (2009) 516–522.
[2] V. Sarin, T.S. Singh, K. Pant, Bioresource. Technol. 97 (2006) 1986–1993.
[3] B. Jiang, Y. Liu, J. Zheng, M. Tan, Z. Wang, M. Wu, Environ. Sci. Technol. 49 (2015) 12363–12371.
[4] W. Jiang, Q. Cai, W. Xu, M. Yang, Y. Cai, D.D. Dionysiou, K.E. O'shea, Environ. Sci. Technol. 48 (2014) 8078–8085.
[5] C. Mondal, M. Ganguly, J. Pal, A. Roy, J. Jana, T. Pal, Langmuir 30 (2014) 4157–4164.
[6] K. Bhowmik, A. Mukherjee, M.K. Mishra, G. De, Langmuir 30 (2014) 3209–3216.
[7] B. Saha, C. Orvig, Coordin. Chem. Rev. 254 (2010) 2959–2972.
[8] H.-L. Ma, Y. Zhang, Q.-H. Hu, D. Yan, Z.-Z. Yu, M. Zhai, J. Mater. Chem. 22 (2012) 5914–5916.
[9] Y. Xing, X. Chen, D. Wang, Environ. Sci. Technol. 41 (2007) 1439–1443.
[10] W. Zheng, J. Hu, Z. Han, Z. Wang, Z. Zheng, J. Langer, J. Economy Chem. Commun. 51 (2015) 9853–9856.
[11] M.N. Kathiravan, R. Karthick, K. Muthukumar, Chem. Eng. J. 169 (2011) 107–115.
[12] C. Desai, K. Jain, D. Madamwar, Bioresour. Technol. 99 (2008) 6059–6069.
[13] G. Bayramoglu, M.Y. Arica, J. Hazard. Mater. 187 (2011) 213–221.
[14] X. Guo, B. Du, Q. Wei, J. Yang, L. Hu, L. Yan, W. Xu, J. Hazard. Mater. 278 (2014) 211–220.
[15] J. Fang, Z. Gu, D. Gang, C. Liu, E.S. Ilton, B. Deng, Environ. Sci. Technol. 41 (2007) 4748–4753.
[16] Z. Ai, L. Zhang, F. Song, Acs. Appl. Mater. Inter. 7 (2015) 1997–2005.
[17] G. Li, F. Qin, R. Wang, S. Xiao, H. Sun, R. Chen, J. Colloid Interface Sci. 409 (2013) 43–51.
[18] W. Liu, J. Ni, X. Yin, Water Res. 53 (2014) 12–25.
[19] A. Lu, S. Zhong, J. Chen, J. Shi, J. Tang, X. Lu, Environ. Sci. Technol. 40 (2006) 3064–3069.
[20] X. Pan, Z. Liu, Z. Chen, Y. Cheng, D. Pan, J. Shao, Z. Lin, X. Guan, Water Res. 55 (2014) 21–29.
[21] Y.-S. Yun, D. Park, J.M. Park, B. Volesky, Environ. Sci. Technol. 35 (2001) 4353–4358.
[22] K. Sundar, A. Mukherjee, M. Sadiq, N. Chandrasekaran, J. Hazard. Mater. 187 (2011) 553–561.
[23] J. Hu, S. Weng, Z. Zheng, Z. Pei, M. Huang, P. Liu, J. Hazard. Mater. 264 (2014) 293–302.
[24] F. Dong, Z. Wang, Y. Li, W.-K. Ho, S. Lee, Environ. Sci. Technol. 48 (2014) 10345–10353.
[25] F. Dong, Z. Zhao, Y. Sun, Y. Zhang, S. Yan, Z. Wu, Environ. Sci. Technol. 49 (2015) 12432–12440.
[26] A. Kleiman, A. Márquez, M. Vera, J. Meichtry, M. Litter, Appl. Catal. B: Environ. 101 (2011) 676–681.
[27] Y. Yang, G. Wang, Q. Deng, D.H. Ng, H. Zhao, Acs. Appl. Mater. Interfaces 6 (2014) 3008–3015.
[28] H. Li, S. Wu, C.-Y. Wu, J. Wang, L. Li, K. Shih, Environ. Sci. Technol. 49 (2015) 7373–7379.
[29] Y. Ku, I.L. Jung, Water Res. 35 (2001) 135–142.
[30] X. Xu, L. Hu, N. Gao, S. Liu, S. Wageh, A.A. Al-Ghamdi, A. Alshahrie, X. Fang, Adv. Funct. Mater. 25 (2015) 445–454.
[31] Z. Chen, S. Liu, M.Q. Yang, Y.J. Xu, Acs. Appl. Mater. Interfaces 5 (2013) 4309–4319.
[32] S. Polisetti, P.A. Deshpande, G. Madras, Ind. Eng. Chem. Res. 50 (2011) 12915–12924.
[33] M. Naimi-Joubani, M. Shirzad-Siboni, J.K. Yang, M. Gholami, M. Farzadkia, J. Ind. Eng. Chem. 22 (2014) 317–323.
[34] M.S. Siboni, M.T. Samadi, J.K. Yang, S.M. Lee, Environ. Technol. 32 (2011) 1573–1579.
[35] Y.C. Zhang, J. Li, M. Zhang, D.D. Dionysiou, Environ. Sci. Technol. 45 (2011) 9324–9331.
[36] J. Wang, X. Li, X. Li, J. Zhu, H. Li, Nanoscale 5 (2013) 1876–1881.
[37] M. Baikousi, A.B. Bourlinos, A. Douvalis, T. Bakas, D.F. Anagnostopoulos, J. i. Tuček, K.R. Šafařířovaí, R. Zboril, M.A. Karakassides, Langmuir 28 (2012) 3918–3930.
[38] L. Li, Z. Zhu, G. Lu, Z. Yan, S. Qiao, Carbon 45 (2007) 11–20.
[39] S. Goswami, A.K. Das, A.K. Maity, A. Manna, K. Aich, S. Maity, P. Saha, T.K. Mandal, Dalton Trans. 43 (2014) 231–239.
[40] H. Wang, X. Zhou, M. Yu, Y. Wang, L. Han, J. Zhang, P. Yuan, G. Auchterlonie, J. Zou, C. Yu, J. Am. Chem. Soc. 128 (2006) 15992–15993.
[41] D. Cabaret, S. Adediran, R. Pratt, M. Wakselman, Biochemistry 42 (2003) 6719–6725.
[42] D.J. Macquarrie, Chem. Commun. (1996) 1961–1962.
[43] M. Shirzad-Siboni, M. Farrokhi, R. Darvishi Cheshmeh Soltani, A. Khataee, S. Tajassosi, Ind. Eng. Chem. Res. (2014) 1079–1087.